Revue des Composites et des Matériaux Avancés-Journal of Composite and Advanced Materials
Vol. 36, No. 1, February, 2026, pp. 145-154
Journal homepage: http://iieta.org/journals/rcma

Enhanced Impact Strength of Polystyrene Composites Reinforced with Binary and Ternary Zn–Cd–Te Fillers

Ibtisam Zaidan Khalaf*, Hadeel Khamees Khalil

Al-Anbar Education Directorate, Ministry of Education, Anbar 31001, Iraq

Corresponding Author Email: hk1991kk@gmail.com

https://doi.org/10.18280/rcma.360114

Received: 10 November 2025
Revised: 28 January 2026
Accepted: 15 February 2026
Available online: 28 February 2026

Keywords:
polystyrene composites, Zn-Cd-Te ternary fillers, synergistic toughening, impact strength, fracture morphology, interfacial adhesion

ABSTRACT

This study investigates the impact resistance of polystyrene (PS) composites reinforced with novel zinc-cadmium-tellurium (Zn-Cd-Te) ternary fillers. Three distinct systems were fabricated: binary Zn_xTe_{1-x}/PS and Zn_xTe_{1-x}/PS/PS, and a ternary Zn_xTe_{1-x}/PS hybrid, incorporating varying filler weight fractions (Ψ). Impact properties were quantified using Charpy and Izod pendulum tests, correlated with fracture surface morphology analyzed via optical microscopy. Results demonstrate that substituting Te with Zn or Cd significantly enhances energy absorption, attributed to improved interfacial adhesion and crack deflection mechanisms. While Zn-based binaries outperformed Cd-based counterparts (2.50 vs. 2.10 kJ/m²) due to finer particle dispersion, the ternary hybrid system exhibited a superior synergistic effect, achieving a peak impact strength of 3.10 kJ/m². A near-linear correlation between filler loading and impact strength was observed across all systems, indicating robust filler-matrix cohesion. These findings confirm that Zn-Cd-Te/PS hybrids offer a strategic advantage over binary systems for developing lightweight, high-toughness structural materials.

1. INTRODUCTION

Polystyrene is widely used as a thermoplastic material owing to its low cost, optical clarity, and ease of processing. Although these advantages are significant, its intrinsic brittleness severely limits its application in areas that require high mechanical toughness. Filler reinforcement in polystyrene (PS) to increase the impact strength of the material has thus become an active topic of research on materials [1-3]. Recent developments have demonstrated that hybrid inorganic-organic and 3D filler systems can greatly improve the thermal stability, tensile strength, and impact resistance of PS, especially when well dispersed within the polymer matrix [4, 5], and emphasize the sustainability, recyclability, and multifunctionality of hybrid PS composites in advanced structural applications [6-8]

Of specific interest are inorganic fillers zinc (Zn), cadmium (Cd), and tellurium (Te) because they possess tunable behavior and have the potential to enhance the adhesion of the filler to the matrix, dissipation of energy, and crack resistance. Among these fillers, Zn-based additives have demonstrated the most significant improvements in mechanical performance. As an example, the addition of silver-modified tetrapod-like ZnO whiskers into PS increased antibacterial performance and impact resistance due to the improvement of dispersion and anchoring properties [9]. Equally, it has been reported that nano-ZnO fillers increase surface hardness by almost 47 percent even at the low concentration of 0.3 wt%, indicating strong particle-matrix compatibility [10]. Subsequent research has validated that Zn-based ionomeric systems and ZnO-based hybrid fillers can enhance toughness and heat resistance and retain processability at the same time, resulting in increased utility of PS composites [11, 12].

Cadmium-based fillers, which have not been investigated extensively due to environmental reasons, have demonstrated promising effects on composite structure upon alloying with Zn and Te. Zn addition to CdTe matrices enhances crystal toughness and decreases the density of dislocations and suggests the synergistic behavior of hybrid systems [13, 14]. Moreover, CdTe and CdS-ZnS hybrid nanocompositions have been discovered to enhance optical and mechanical properties owing to homogenous nanoparticle dispersion and compatibility with matrices, which appears to underscore the ability of Cd- and Te-based systems to make multifunctional PS composites [15, 16].

Recent studies further support the advantages of Zn fillers in PS composites. Wacharawichanant et al. [17] also established that the use of a compatibilizer like styrene-maleic anhydride can further be used to enhance mechanical properties, increasing ZnO dispersion and particle-polymer interaction. Similarly, the study [18] demonstrated that tensile strength and elongation at break of PS composites steadily increase with ZnO content to 7 wt% (which is reinforcing), meaning that it can enhance strength despite higher loads. It has also been complemented by other studies that hybridization of ZnO with carbonaceous or biochar fillers enhances interfacial bonding, impact strength, and fracture resistance by synergistic energy dissipation processes [19, 20].

Hybrid Zn/Cd filler systems have also attracted interest due to their improved resistance to environmental degradation and radiation. To illustrate, a recent study on polypropylene composites discovered that CdS-ZnS fillers drastically reduced the formation of free radicals during gamma irradiation, which indicated radiation stability, which is a desirable property when used in structural applications [21]. Additionally, hybrid fillers based on the combination of nanoclays, red mud, or metallic oxides with PS have demonstrated higher toughness and flame retardancy, promoting the general applicability of multi-filler design strategies [22, 23].

In spite of these encouraging developments, an extensive literature has not yet compared the effect strength of PS composites reinforced by binary and ternary systems of Zn, Cd and Te under their standard preparation and testing conditions. The current study fills this gap by covering the substitutional effects and synergetic reinforcement processes in Zn-Te, Cd-Te and Zn-Cd-Te systems. The test of standardized impact testing and fracture morphology will serve to clarify the relationship between particle characteristics and filler synergy and toughness in PS composites.

2. MATERIALS AND METHODS

2.1 Materials

PS resin was selected as the polymeric matrix due to its transparency, availability, and broad spectrum of industrial uses. Three inorganic powders were added to the matrix to strengthen it, namely, Zn, Cd and Te. These powders differed in particle size and mechanical durability, which are critical parameters affecting filler-matrix interactions. Zinc had the smallest average particle size of approximately 50 μm and exhibited the highest durability, cadmium had an intermediate grain size of 60 μm and moderate durability, while tellurium had the largest grain size of 76 μm and was considered the least durable. These intrinsic differences were expected to influence the fracture resistance of the composites.

2.2 Composite preparation

Three sets of PS-based composites were prepared by incorporating Zn, Cd, and Te powders in controlled weight fractions (Ψ). In each group, the total filler fraction was held constant, while the relative proportions of the constituent reinforcing elements were systematically varied. This design ensured that the effects of progressive substitution could be clearly investigated.

At each weight fraction, six distinct samples (No. 1-6) were fabricated. Sample No. 1 corresponded to the composition with the maximum Te (or Cd in Group 3) content and no Zn, whereas Sample No. 6 corresponded to the opposite case, with maximum Zn and no Te (or no Cd in Group 3). The intermediate samples (Nos. 2-5) represented stepwise substitutions between the two extremes, with Zn incrementally increasing and Te (or Cd) correspondingly decreasing so that the overall filler content remained constant.

Group G1 (Zn_xTe_{1-x}/PS): The PS content was fixed at 96%, 92%, and 88% for Ψ1 = 4%, Ψ2 = 8%, and Ψ3 = 12%, respectively. Substitution involved replacing Te with Zn.

Group G2 (Cd_xTe_{1-x}/PS): The PS content was again fixed at 96%, 92%, and 88% for Ψ1 = 4%, Ψ2 = 8%, and Ψ3 = 12%. Substitution involved replacing Te with Cd.

Group G3 ($Zn_xCd_{1-x}Te$/PS): For this ternary system, Te was fixed at 2% for all samples, while the remaining filler fraction consisted of varying ratios of Zn and Cd. PS content was reduced to 94%, 90%, and 86% for Ψ1 = 6%, Ψ2 = 10%, and Ψ3 = 14%, respectively. Substitution involved replacing Cd with Zn.

The full set of compositions for all groups is summarized in Table 1, where Samples 1-6 at each Ψ represent the progression from maximum Te (or Cd) to maximum Zn content. The detailed weight fractions of Zn, Cd, Te, and PS for each sample in Groups G1-G3 are provided in Table S1 (Supplementary Material), where the stepwise substitution schemes are shown explicitly for all filler levels.

Table 1. Compositions of prepared composites in Groups G1, G2, and G3

Group	Total Filler Content (Ψ, wt%)	PS Content (wt%)	Sample No.	Filler Composition	Substitution Scheme
G1(Zn_xTe_{1-x}/PS)	4, 8, 12	96, 92, 88	1-6	Zn (0 → 100%) + Te (100 → 0%)	Stepwise replacement of Te with Zn (equal increments at each Ψ)
G2(Cd_xTe_{1-x}/PS)	4, 8, 12	96, 92, 88	1-6	Cd (0 → 100%) + Te (100 → 0%)	Stepwise replacement of Te with Cd (equal increments at each Ψ)
G3($Zn_xCd_{1-x}Te$/PS)	6, 10, 14	94, 90, 86	1-6	Te fixed at 2%; Zn (0 → max) + Cd (max → 0)	Stepwise replacement of Cd with Zn while Te constant

Note: polystyrene (PS); zinc (Zn); cadmium (Cd); tellurium (Te).

2.3 Impact strength testing

The mechanical performance of the composites was examined using pendulum-based impact testing according to Charpy and Izod principles. In the Charpy configuration, the sample was mounted horizontally with a U- or V-shaped notch facing away from the pendulum, whereas in the Izod configuration, the sample was mounted vertically with the notch facing the pendulum. In both cases, the pendulum was raised to a fixed height and released, striking the specimen and transferring a portion of its kinetic energy until fracture occurred. The absorbed energy U (J) was calculated as the difference between the initial and final potential energies of the pendulum according to the relation [24]:

$$U = WR_P(\cos\beta - \cos\alpha) \quad (1)$$

where, W represents the pendulum weight (N), Rp the distance (m) from the pendulum's center of gravity to its rotation axis, and α and β the fall and rise angles, respectively. The impact strength of the specimen was then determined using the formula [25]:

$$I.S = \frac{U}{A} \quad (2)$$

where, A denotes the cross-sectional area (m^2) of the test specimen. This relationship expresses the resistance of the material to fracture under sudden loading as the energy absorbed per unit area.

2.4 Microscopy testing

In addition to mechanical testing, optical microscopy was employed to evaluate the morphology of the composites both before and after impact testing. Samples were observed at magnifications of 50× and 5×, depending on the group under study. Special attention was given to the fracture surfaces, where features such as crack initiation and propagation, matrix tearing, shear bands, and tensile collapse were examined. These microscopic observations provided direct evidence of the reinforcing role of Zn, Cd, and Te fillers, particularly in terms of their ability to hinder crack propagation and improve energy absorption through particle-matrix bonding.

2.5 Experimental procedure

In practice, the experimental process was carried out under a clearly defined sequential protocol. Mixing was performed using a laboratory mechanical stirrer (IKA RW 20 digital, Germany) equipped with a stainless-steel impeller. In the first step, polystyrene (PS) resin was mechanically mixed with Zn, Cd, and Te powders of known grain size at a constant stirring speed of 600 rpm for 20 min to ensure homogeneous dispersion of the fillers. Mixing was conducted at an elevated temperature of approximately 80°C to reduce melt viscosity and promote uniform particle distribution within the polymer matrix.

After mixing, the composite blends were poured into preheated rectangular steel molds (100 × 10 × 4 mm³) and subjected to hot-press molding using a hydraulic hot press (Carver Model 3851, USA) at 150°C under a pressure of 5 MPa for 10 min. The molded specimens were allowed to cool naturally to room temperature before demolding. Standardized impact specimens conforming to Charpy and Izod dimensions were prepared by precision cutting to ensure dimensional uniformity across all samples.

Charpy and Izod impact tests were conducted on separate but identically prepared specimens, rather than on the same specimen, in accordance with standard impact testing practice. This was implemented due to the fact that Charpy and Izod set-ups would not need the same specimen mounting positions and notch loading conditions, which otherwise would cause damage and invalidate the future measurements. The independent specimen was used to provide strong and consistent impact strength values in each testing configuration. Fracture energy and impact strength were determined from the absorbed energy per unit cross-sectional area.

Finally, optical microscopy was performed on selected specimens before and after impact testing to examine fracture morphology and to correlate the observed microstructural features with the measured impact behavior. This controlled experimental design ensured reproducibility, minimized processing-related variability, and enabled reliable comparison among all filler systems and weight fractions.

2.6 Statistical analysis

A statistical test was used to compare the effects of the impact strength between the composite groups. All the data of impact strength are expressed as the mean standard deviation with reference to three independent specimens of the composition (n = 3).

One-way analysis of variance (ANOVA) was utilized to test the mean impact strength values of G1, G2, and G3 at the maximum filler content. In cases where statistically significant differences were observed, post-hoc comparisons were conducted using the honestly significant difference (HSD) test of Tukey.

The statistical significance was established at a confidence of 95% ($p < 0.05$). Standard scientific data analysis software was used to perform all the statistical calculations.

3. RESULTS AND DISCUSSION

3.1 Impact strength of Group G1 (Zn–Te/PS composites)

The results of the impact strength test for Group G1 (Zn–Te/PS composites) are presented in Table 2 and illustrated comparatively in Figure 1. At the lowest weight fraction (Ψ1 = 4%), the impact strength increased from 0.68 kJ/m² for the sample containing only Te and gradually increased with higher Zn content, reaching 2.0 kJ/m² when Te was fully substituted by Zn. A similar behavior was observed at Ψ2 = 8%, where values increased from 1.0 kJ/m² to 2.2 kJ/m² across the substitution range. At Ψ3 = 12%, the trend was even more pronounced, with impact strength rising from 1.33 kJ/m² at 12% Te to a maximum of 2.5 kJ/m² at 12% Zn (Figures 1-6).

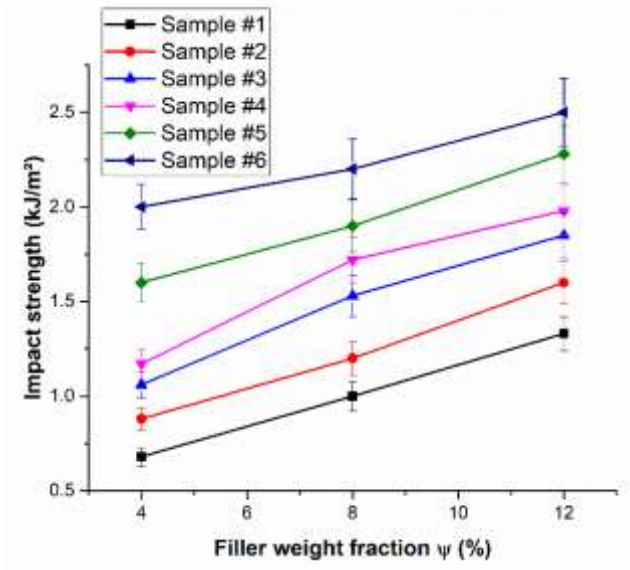

Figure 1. Comparative impact strength of (Zn_xTe_{1-x})/PS composites at different filler weight fractions (Ψ_1 = 4%, Ψ_2 = 8%, Ψ_3 = 12%). Each colored bar represents Samples 1-6 corresponding to increasing Zn substitution (0 → 100%)

These results demonstrate that increasing Zn content at the expense of Te significantly improves the impact resistance of PS composites. Zinc reinforcement is more effective than tellurium due to several factors: (i) its smaller particle size (50 μm compared with 76 μm for Te), which enables Zn to fill voids between PS chains more efficiently, enhancing particle-matrix cohesion; (ii) its higher intrinsic durability, which allows Zn to withstand greater stresses; and (iii) its ability to promote tighter chain packing and cross-linking, thereby

restricting crack propagation. In addition, the relatively high molecular weight of PS (100,000-400,000) enhances toughness, while strong cohesive interactions between Zn and the polymer chains further improve energy absorption.

The comparative plot in Figure 1 confirms that the impact strength increases nearly linearly with both increasing Zn substitution and increasing filler weight fraction. The highest value of 2.5 kJ/m² was obtained at Ψ3 = 12% Zn, which is almost four times higher than the lowest value recorded at Ψ1 = 4% Te. This behavior indicates that Zn fillers play a crucial role in redistributing applied stress and hindering crack propagation, thus substantially improving the toughness of PS-based composites.

Table 2. Impact strength values for G1 (Zn_xTe_{1-x}/PS) at different weight fractions

Sample No.	Ψ1 = 4 wt% (96 wt% PS)	Ψ2 = 8 wt% (92 wt% PS)	Ψ3 = 12 wt% (88 wt% PS)
1	0.68 ± 0.05	1.00 ± 0.08	1.33 ± 0.09
2	0.88 ± 0.06	1.20 ± 0.09	1.60 ± 0.11
3	1.06 ± 0.07	1.53 ± 0.11	1.85 ± 0.12
4	1.17 ± 0.08	1.72 ± 0.12	1.98 ± 0.13
5	1.60 ± 0.10	1.90 ± 0.14	2.28 ± 0.15
6	2.00 ± 0.12	2.20 ± 0.16	2.50 ± 0.18

Note: Values expressed in kJ/m²; polystyrene (PS).

3.2 Impact strength of Group G2 (Cd–Te/PS composites)

The impact strength results for Group G2 (Cd–Te/PS composites) are summarized in Table 3 and comparatively illustrated in Figure 2. At the lowest weight fraction (Ψ1 = 4%), the impact strength increased modestly from 0.68 kJ/m² for the composition with 4% Te to 1.50 kJ/m² when Te was completely replaced by Cd. A similar trend was observed at Ψ2 = 8%, where values rose from 1.0 kJ/m² at full Te content to 1.92 kJ/m² at full Cd substitution. At Ψ3 = 12%, the impact strength values ranged from 1.33 kJ/m² for the Te-rich composition to a maximum of 2.10 kJ/m² for the Cd-rich composite.

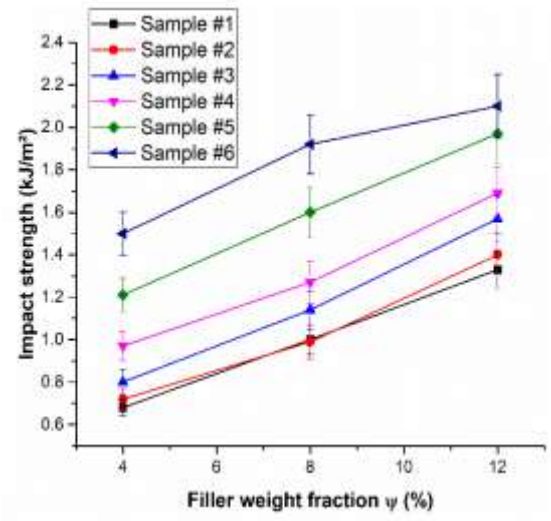

Figure 2. Comparative impact strength of (Cd_xTe_{1-x})/PS composites at different weight fractions (Ψ_1 = 4%, Ψ_2 = 8%, Ψ_3 = 12%)

Compared with G1, the results demonstrate that cadmium reinforcement is less effective than zinc in enhancing the impact strength of PS composites. This is attributed primarily to differences in physical properties: the grain size of Cd (60 μm) is larger than that of Zn (50 μm) but smaller than Te (76 μm), which allows it to fill voids between PS chains better than Te but less efficiently than Zn. Additionally, cadmium possesses lower intrinsic durability than zinc, which reduces its ability to redistribute stress and resist crack propagation. As a result, Cd-reinforced samples generally exhibited lower energy absorption values than their Zn counterparts.

Nevertheless, a consistent improvement was observed with increasing Cd substitution and filler content. The maximum recorded value of 2.10 kJ/m² at Ψ3 = 12% Cd was higher than the corresponding Te-rich composition but remained significantly below the maximum of 2.50 kJ/m² obtained with Zn in G1. This confirms that while cadmium contributes positively to impact resistance compared with tellurium, its reinforcing effect is inferior to that of zinc. The comparative plot (Figure 2) highlights this behavior, showing a gradual but weaker slope compared with the Zn-Te system.

Table 3. Impact strength values for G2 (Cd_xTe_{1-x}/PS) at different weight fractions

Sample No.	Ψ1 = 4 wt% (96 wt% PS)	Ψ2 = 8 wt% (92 wt% PS)	Ψ3 = 12 wt% (88 wt% PS)
1	0.68 ± 0.04	1.00 ± 0.07	1.33 ± 0.09
2	0.72 ± 0.05	0.99 ± 0.08	1.40 ± 0.10
3	0.80 ± 0.06	1.14 ± 0.09	1.57 ± 0.11
4	0.97 ± 0.07	1.27 ± 0.10	1.69 ± 0.12
5	1.21 ± 0.08	1.60 ± 0.12	1.97 ± 0.14
6	1.50 ± 0.10	1.92 ± 0.14	2.10 ± 0.15

Note: Values expressed in kJ/m²; polystyrene (PS).

3.3 Impact strength of Group G3 (Zn–Cd–Te/PS composites)

Group G3 consisted of ternary Zn–Cd–Te/PS composites in which tellurium content was fixed at 2% while the PS content was reduced to 94%, 90%, and 86% for Ψ1 = 6 wt%, Ψ2 = 10 wt%, and Ψ3 = 14 wt%, respectively. The results are summarized in Table 4 and shown comparatively in Figure 3. At Ψ1 = 6 wt%, the impact strength increased from 1.55 kJ/m² for the Cd-rich composition to 2.24 kJ/m² for the Zn-rich composition. At Ψ2 = 10%, the trend was more pronounced, with values rising from 1.95 kJ/m² to 2.71 kJ/m² across the substitution range. At Ψ3 = 14%, the impact strength reached its highest values, ranging from 2.66 kJ/m² to a maximum of 3.10 kJ/m².

These findings demonstrate that combining Zn and Cd in the presence of a fixed 2% Te significantly enhances the toughness of PS composites. The improvement can be attributed to the favorable physical properties of Zn and Cd compared with Te. Both Zn and Cd have smaller grain sizes (50 μm and 60 μm, respectively) than Te (76 μm), which allows them to penetrate the polymer matrix more effectively and hinder crack propagation. In addition, the coexistence of Zn and Cd likely promotes complementary reinforcement: Zn provides strong mechanical anchoring due to its smaller size and higher hardness, while Cd contributes ductility that mitigates localized stress concentration. This dual behavior improves load transfer and delays crack propagation. The optical micrographs (Figure 6(b)) support this mechanism—tortuous crack paths and plastic shear zones observed in G3 correspond to its highest impact strength (3.10 kJ/m²). This

leads to higher absorbed energy and greater impact strength than in the binary systems of G1 and G2.

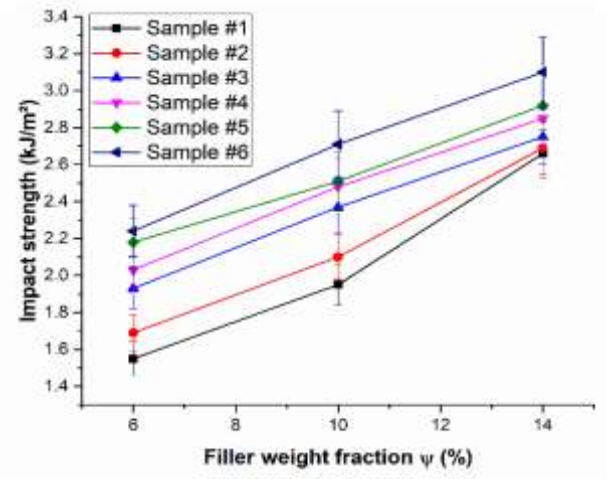

Figure 3. Comparative impact strength of (Zn_xTeCd_{1-x})/PS composites at different weight fractions (Ψ_1 = 6%, Ψ_2 = 10%, Ψ_3 = 14%)

Table 4. Impact strength values for Group G3 (Zn_xTeCd_{1-x}/PS) at different weight fractions

Sample No.	Ψ1 = 6 wt% (94 wt% PS)	Ψ2 = 10 wt% (90 wt% PS)	Ψ3 = 14 wt% (86 wt% PS)
1	1.55 ± 0.09	1.95 ± 0.11	2.66 ± 0.13
2	1.69 ± 0.10	2.10 ± 0.12	2.69 ± 0.14
3	1.93 ± 0.11	2.37 ± 0.14	2.75 ± 0.15
4	2.03 ± 0.12	2.48 ± 0.15	2.85 ± 0.16
5	2.18 ± 0.13	2.51 ± 0.16	2.92 ± 0.17
6	2.24 ± 0.14	2.71 ± 0.18	3.10 ± 0.19

Note: Values expressed in kJ/m²; polystyrene (PS).

3.4 Comparative discussion of Groups G1, G2, and G3

A comparison of the three groups provides valuable insight into the relative reinforcing efficiency of Zn, Cd, and Te in polystyrene composites. As shown in Tables 1-4 and the corresponding comparative figures, all systems exhibited a progressive increase in impact strength with increasing filler content, reflecting the general effectiveness of particulate reinforcement in enhancing the toughness of PS. However, the magnitude of improvement was strongly dependent on the type and combination of fillers.

G1, reinforced with Zn and Te, displayed the highest performance among the binary systems, with impact strength values ranging from 0.68 kJ/m² at Ψ1 (Te-rich) to a maximum of 2.50 kJ/m² at Ψ3 (Zn-rich). In contrast, Group G2, composed of Cd-Te/PS composites, achieved a maximum of only 2.10 kJ/m², which was consistently lower than the corresponding Zn-Te compositions. This can be attributed to the smaller particle size (50 μm) and higher intrinsic durability of Zn compared with Cd (60 μm), which promote better filler-matrix interaction and crack resistance.

The ternary system (Group G3) where Zn and Cd were used with a fixed 2% Te content gave the highest overall performance with the highest impact strength of 3.10 kJ/m^2 at the PS3. It is much higher than the maxima of G1 and G2, indicating a definite synergistic effect of the inclusion of Zn and Cd in combination. The presence of both Zn and Cd is likely to facilitate better stress transfer, decrease voids in the polymer framework and inhibit crack propagation in a number of ways. This increases ductility and toughness and counters the lower reinforcing efficiency of Te.

The observed variations between Groups G1, G2, and G3 at the highest filler content are reflected in the corresponding standard deviation values (n = 3 per composition). The average impact strength of the ternary ZnCdTe/PS system (G3) is higher than the binary systems (G1 and G2) with limited overlap in the variability, indicating a statistically significant enhancement in impact resistance ($p < 0.05$). This phenomenon indicates strongly that the increased performance of G3 does not occur due to experimental scatter but due to the synergistic effect of Zn and Cd fillers with the PS matrix.

A one-way ANOVA of the obtained impact strength of the filler content (G1, G2, and G3) at the maximum filler content (ψ3) was performed to quantitatively approve the observations. The statistical analysis revealed a significant difference among the three groups, with $F(2, 15) = 21.56$ and an exact p-value of 3.87×10^{-5}. This finding proves that the high impact strength of the ternary Zn -Cd-Te/PS system has a significant statistical significance and cannot be explained by scattering in the experiment. The significantly improved performance of Group G3 thus indicates a real synergistic reinforcing efficiency due to the combined contribution of Zn and Cd fillers in the polystyrene matrix.

The comparative results lead to three key observations. To begin with, Zn is a better reinforcing material than Cd with Te since it has a smaller grain size and higher intrinsic durability. Second, the fraction of filler weight systematically increases the impact strength of all the groups; the increase rate is, however filler-dependent. Third, the hybrid reinforcement mechanism of G3 gives the best performance because the combination of Zn and Cd has complementary characteristics, which leads to a higher fracture energy absorption of the hybrid system compared with the binary systems.

Collectively, these results validate that the ternary Zn-Cd-Te/PS system is the best formulation, which integrates high impact resistance, good distribution of fillers, and good bonding of fillers and the matrix. The results affirm that ternary ZnCdTe/PS composites exhibit optimal impact performance because of synergistic redistribution of stress and increased capacity of fracture energy. Nevertheless, the environmental and health risks of cadmium ought to be closely taken into account in further design, promoting the use of less toxic analogues.

3.5 Optical microscopy analysis of impacted samples

The optical microscopy was used to study the surface morphology of composite samples prior to and after impact testing. The method offers information on the integrity of the polymer matrix, the reinforcement dispersion quality, and failure mechanisms that take place under sudden loading. The descriptive images of each group (G1, G2, and G3) are discussed below.

3.5.1 G1

The G1 sample optical image before the test (see Figure 4) showed a rather smooth and homogeneous surface morphology. The resin matrix looked straight without any visible microcracks, pores or delamination areas. This was a sign of a good polymerization of the matrix and sufficient adhesion between the chains of polymer.

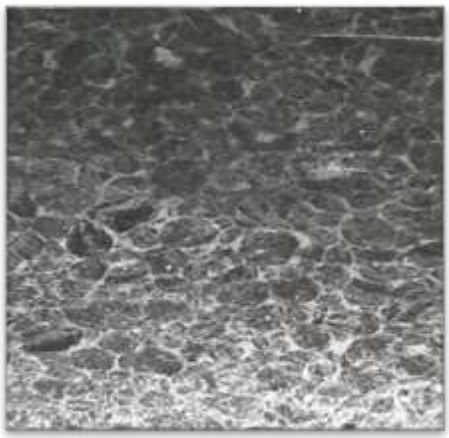

(a) Before impact

(b) After impact

Figure 4. Surface morphology of G1

(a) Before impact

(b) After impact

Figure 5. Surface morphology of G2

The examination of a post-impact displayed the formation of several cracks, as well as local delamination. The fracture face was rough, pointing out to the dissipation of energy by way of matrix cracking. Brittle fracture was the leading failure mode, which indicated that the G1 formulation had a low plastic deformation capacity when subjected to dynamic loading.

3.5.2 G2

The pre-impact surface of G2 (see Figure 5) showed a more textured appearance compared to G1. Minor anomalies indicated subtleties of resin homogeneity, which might have existed due to the differences in the filler dispersion or curing shrinkage. Nonetheless, the matrix appeared largely intact.

After the impact event, the G2 sample displayed distinctive layered fracture patterns. The surface morphology revealed shear cracks running along the loading direction, accompanied by regions of resin pull-out. The higher surface roughness compared to G1 indicates enhanced energy absorption capacity, as the irregular fracture propagation path required more energy to develop. This suggests that G2 may exhibit better impact resistance relative to G1.

3.5.3 G3

The optical image of G3 before impact (see Figure 6) showed a relatively uniform distribution of the resin phase with a reflective texture. Compared to G1 and G2, the microstructure appeared denser and less porous, suggesting stronger molecular packing or improved filler-matrix interfacial bonding.

(a) Before impact

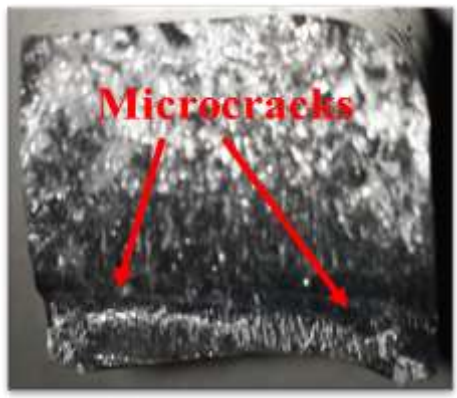

(b) After impact

Figure 6. Surface morphology of G3

Following impact, the G3 sample revealed a highly rough and irregular fracture surface. Clear signs of matrix plastic deformation and shear band formation were observed, along with fragmented resin clusters adhering to the fracture edges. The presence of tortuous crack paths indicates that the impact

energy was dissipated through multiple mechanisms, including crack deflection, plastic flow, and micro-fracturing. Among the three groups, G3 displayed the highest fracture surface roughness, which is typically correlated with improved toughness and superior impact resistance. These tortured crack paths and plastic shear zones are effective energy-dissipation processes since they cause the propagating crack to change direction and experience localized plastic deformation multiple times. Consequently, more impact energy is absorbed until final fracture, a fact that directly explains the high impact strength values obtained in G3 (3.10 kJ/m^2) relative to the binary systems. Other high-toughness polymer composites have exhibited similar toughening mechanisms, involving crack deflection, plastic shear banding, and localized deformation at filler-matrix interfaces, with multi-scale crack deviation and microplasticity emerging as key energy-dissipating behaviors [26-30]. Studies on filled and hybrid composites further demonstrate that shear yielding, crack deflection, and interfacial debonding collectively increase energy absorption and delay catastrophic fracture [31].

3.6 Comparative discussion

A comparative assessment of G1, G2, and G3 reveals a progressive improvement in impact energy dissipation mechanisms:

- G1 exhibited a predominantly brittle fracture with minimal roughness, reflecting its limited capacity to resist sudden loading.
- G2 demonstrated enhanced surface irregularity and layered fracture patterns, suggesting improved toughness due to shear cracking and energy-absorbing mechanisms.
- G3 displayed the most pronounced roughness and deformation features, highlighting its superior ability to dissipate impact energy through plastic flow, crack deflection, and micro-fragmentation.

These findings confirm that the material formulation used in G3 is most effective in enhancing impact resistance, followed by G2, while G1 is the weakest in this regard. The series of post impact images with rising surface roughness has been a direct indication of enhanced fracture toughness.

4. CONCLUSIONS

In this research, the impact strength of polystyrene (PS) composites strengthened with Zn, Cd, and Te in binary and ternary fillers based on weight fraction was investigated. The overall findings can be summarized as follows:

Effect of filler substitution: The reinforcing efficiency of metallic fillers was proved by the consistent improvement in impact strength of PS composites when Te was replaced by Zn or Cd.

Zinc superiority: Zn-Te/PS composites (G1) demonstrated superior performance compared with Cd-Te/PS composites (G2), reaching maximum impact strengths of 2.50 kJ/m² and 2.10 kJ/m², respectively. The higher reinforcing capability of Zn is attributed to its smaller particle size (50 μm) and greater intrinsic durability relative to Cd.

Synergistic ternary effect: The ternary Zn-Cd-Te/PS system (G3) exhibited the highest impact resistance, achieving a maximum of 3.10 kJ/m², thereby surpassing both binary counterparts. The combined presence of Zn and Cd facilitated stress redistribution and reduced crack propagation, resulting in a synergistic toughening effect.

Influence of weight fraction: For all composite systems, impact strength increased almost linearly with filler content (Ψ), reflecting improved filler-matrix cohesion and more efficient particle dispersion.

Practical implications: Hybrid filler systems outperformed single-filler composites in fracture resistance, suggesting that Zn-Cd-Te/PS composites are promising candidates for lightweight applications where enhanced toughness and durability are critical.

While the findings highlight significant improvements in impact strength, several limitations must be noted. The study was confined to impact strength measurements, without considering other essential mechanical properties such as tensile, compressive, or flexural behavior. Furthermore, only optical microscopy was employed for microstructural analysis, which limited the resolution in capturing detailed particle-matrix interactions. The particle sizes were also fixed (Zn: 50 μm, Cd: 60 μm, Te: 76 μm), leaving the influence of finer (nano-scale) or coarser particles unexplored.

Future research should broaden the scope to encompass a wider range of mechanical and thermal characterizations, supported by advanced techniques such as scanning electron microscopy (SEM), transmission electron microscopy (TEM), and X-ray diffraction (XRD). Investigating the role of particle size variation, surface modifications, and optimized filler ratios would provide deeper insights into tailoring filler-matrix interactions. Additionally, long-term studies addressing fatigue performance, environmental stability, and aging behavior are essential for validating the real-world applicability of these composites in structural and functional components.

GENERATIVE AI STATEMENT AND CONFLICT OF INTEREST

The use of generative AI tools was limited to language corrections and structural editing of the manuscript. Scientific data, results, and the development of the core scientific material were generated with no AI tools. The authors alone are in charge of all scientific interpretations and conclusions.

The authors state that they do not have any recognized conflicting financial interests or personal relationships that might have emerged to affect the work in this paper. This study did not receive any external funding.

REFERENCES

[1] Sahai, R.S.N., Pardeshi, R.A. (2021). Comparative study of effect of different coupling agent on mechanical properties and water absorption on wheat straw-reinforced polystyrene composites. Journal of Thermoplastic Composite Materials, 34(4): 433-450. https://doi.org/10.1177/0892705719843975

[2] Xu, H., Sun, Y., Song, G., Song, Y., et al. (2023). The mechanical properties of polystyrene composites were improved by designing large-size 3D GO/CNTs hybrid aerogel reinforced by epoxy resin. Journal of Applied Polymer Science, 140(33): e54284. https://doi.org/10.1002/app.54284

[3] Ponsoni, L.V., de Almeida, M.K., Madeira, K., Militão,

G.P., Zimmermann, M.V.G. (2024). Statistical analysis of the substitution of inorganic fibers and fillers with vegetable fibers and fillers in polystyrene composites. Journal of Applied Polymer Science, 141(24): e55497. https://doi.org/10.1002/app.55497

[4] Ladavos, A., Giannakas, A.E., Xidas, P., Giliopoulos, D.J., et al. (2021). Preparation and characterization of polystyrene hybrid composites reinforced with 2D and 3D inorganic fillers. Micro, 1(1): 3-14. https://doi.org/10.3390/micro1010002

[5] Bulanda, K., Oleksy, M., Oliwa, R. (2022). Hybrid polymer composites based on polystyrene (PS) used in the melted and extruded manufacturing technology. Polymers, 14(22): 5000. https://doi.org/10.3390/polym14225000

[6] Zhang, J., Liu, H., Sablani, S.S., Wu, Q. (2024). Recycling functional fillers from waste tires for tailored polystyrene composites: Mechanical, fire-retarding, electromagnetic field shielding, and acoustic insulation properties—A short review. Materials, 17(11): 2675. https://doi.org/10.3390/ma17112675

[7] Capricho, J.C., Prasad, K., Hameed, N., Nikzad, M., Salim, N. (2022). Upcycling polystyrene. Polymers, 14(22): 5010. https://doi.org/10.3390/polym14225010

[8] Alshammari, B.A., Alenad, A.M., Al-Mubaddel, F.S., Alharbi, A.G., et al. (2022). Impact of hybrid fillers on the properties of high density polyethylene based composites. Polymers, 14(16): 3427. https://doi.org/10.3390/polym14163427

[9] Pan, X., Peng, L., Liu, Y., Wang, J. (2014). Highly antibacterial and toughened polystyrene composites with silver nanoparticles modified tetrapod-like zinc oxide whiskers. Journal of Applied Polymer Science, 131(20): 40862. https://doi.org/10.1002/app.40900

[10] Alam, M.A., Ya, H.H., Hussain, P.B., Azeem, M., Sapuan, S.M., khan, R., Ahamad, T. (2020). Experimental investigations on the surface hardness of synthesized polystyrene/ZnO nanocomposites. Materials Today: Proceedings, 33: 345-352. https://doi.org/10.1007/978-981-15-5753-8_32

[11] Song, Z., Wang, J., Tao, Q., Yu, Y., et al. (2022). Zn-salt poly (styrene–ran–cinnamic acid) ionomer as a polystyrene with improved impact toughness, heat resistance, and minimally compromised processability. Journal of Applied Polymer Science, 138(41): 52041. https://doi.org/10.1002/app.52041

[12] Abdalla, T.N., Hasan, A.F., Hashim, A.A. (2022). Characterization of mechanical and electrical properties of polystyrene composite reinforced by hybrid reinforcement filler. Diyala Journal of Engineering Sciences, 15(3): 42-52. https://doi.org/10.24237/djes.2022.15305

[13] McDevitt, S., Dean, B.E., Ryding, D.G., Scheltens, F.J., Mahajan, S. (1986). Characterization of CdTe and (Cd, Zn) Te single-crystal substrates. Materials Letters, 4(11-12): 451-454. https://doi.org/10.1016/0167-577X(86)90035-2

[14] Tedjini, M.H., Oukebdane, A., Belkaid, M.N., Aouail, N. (2021). The effect of zinc concentration upon electronic structure, optical and dielectric properties of $Cd_{1-x}Zn_xTe$ alloy: TB-mBJ investigation. Computational Condensed Matter, 27: e00561. https://doi.org/10.1016/j.cocom.2021.e00561

[15] Wu, G., Zhou, L., Yan, S., Xia, X., Xiong, Y., Xu, W. (2011). Transparent, fluorescent, and mechanical enhanced elastomeric composites formed with poly (styrene-butadiene-styrene) and SiO2-hybridized CdTe quantum dots. Journal of Applied Polymer Science, 122(4): 2325-2330. https://doi.org/10.1002/app.34370

[16] Li, G., Fan, G.L., Fan, Y.L., Jiang, J.Q., Shi, X.Y., Liu, Z.W. (2022). Polystyrene-poly (ethylene-butylene)-polystyrene/asphaltene sands composite elastomer with improved mechanical properties. Journal of Applied Polymer Science, 139(7): 51637. https://doi.org/10.1002/app.51637

[17] Wacharawichanant, S., Saetun, P., Lekkong, T., Thongyai, S., Praserthdam, P. (2012). Effect of poly(styrene-co-maleic anhydride) compatibilizer on properties of polystyrene/zinc oxide composites. Iranian Polymer Journal, 21(6): 385-396. https://doi.org/10.1007/s13726-012-0041-2

[18] Rehman, S., Javaid, S., Shahid, M., Gul, I., Rashid, B., Szczepanski, C.R., Naveed, M., Curley, S.J. (2022). Polystyrene–Sepiolite Clay Nanocomposites with Enhanced Mechanical and Thermal Properties. Polymers, 14(17): 3576. https://doi.org/10.3390/polym14173576

[19] Adeniyi, A.G., Abdulkareem, S.A., Adeyanju, C.A., Abdulkareem, M.T., et al. (2023). Mechanical and morphological analyses of flamboyant seed pod biochar/aluminium filings reinforced hybrid polystyrene composite. Journal of the Indian Academy of Wood Science, 20(1): 28-36. https://doi.org/10.1007/s13196-023-00311-4

[20] Adeniyi, A.G., Abdulkareem, S.A., Emenike, E.C., Abdelbacki, A.M., et al. (2024). Mechanical and chemical characterization of biochar-reinforced polystyrene composites. BMC Chemistry, 18(1): 246. https://doi.org/10.1186/s13065-024-01365-2

[21] Gurbanov, M.A., Hajieva, Y.G., Gasimov, R.J., Bayramov, M.A., Mustafayev, I.I. (2024). EPR Study of the effect of γ-irradiation on polypropylene/(CdS+ ZnS) composites. Problems of Atomic Science and Technology, 4: 29-33. https://doi.org/10.46813/2024-152-029

[22] Ajayi, A.A., Turup Pandurangan, M., Kanny, K. (2023). Influence of hybridizing fillers on mechanical properties of foam composite panel. Polymer Engineering & Science, 63(8): 2565-2577. https://doi.org/10.1002/pen.26396

[23] Özmeral, N., Soydal, U., Kocaman, S., Ahmetli, G. (2023). Red mud waste/nanoclay/polystyrene-modified epoxy hybrid composites: Mechanical, thermal, and flammability properties. Journal of Applied Polymer Science, 140(31): e54218. https://doi.org/10.1002/app.54218

[24] Unal, M., Dalmış, İ. (2022). A prototype Charpy and Izod impact tester design and impact test analysis of different aluminum alloys. Journal of the Technical University of Gabrovo, 65: 32-37. https://doi.org/10.62853/DOTY3194

[25] Boangmanalu, E.P.D., Pratama, A.B., Qadry, A., Saragi, J.F.H., Sinaga, F.T.H. (2023). Charpy and izod method impak strength analysis on st 37 steel with temperature variations. Formosa Journal of Science and Technology, 2(12): 3329-3342. https://doi.org/10.55927/fjst.v2i12.7074

[26] Huang, Y., Wei, Y., Huang, C., Qiu, Y., Gu, B., Yang,

B. (2025). Overcoming low-polarity limitations in polyphenylene oxide electrospinning: Chemical functionalization and polymer hybridization for interlaminar toughening of carbon fiber composites. Polymers, 17(11): 1480. https://doi.org/10.3390/polym17111480

[27] Song, L., Wang, W., Chen, D., Ren, J., et al. (2023). Controllable synthesis of submicrometer core–shell modifier and its effect on toughening polypheylene ether/polystyrene blends. Macromolecular Materials and Engineering, 308(4): 2200537. https://doi.org/10.1002/mame.202200537

[28] Zhu, L.D., Yang, H.Y., Cai, G.D., Zhou, C., et al. (2013). Submicrometer-sized rubber particles as "craze-bridge" for toughening polystyrene/high-impact polystyrene. Journal of Applied Polymer Science, 129(1): 224-229. https://doi.org/10.1002/app.38716

[29] Zhang, H., Li, Y., Jiang, N., Zhou, N., et al. (2025). Strength and toughness: Multi-particle synergism imparts rigid-toughness balance to poly(ether-ether-ketone) composites. Polymer Composites, 46(12): 13416-13432. https://doi.org/10.1002/pc.29939

[30] Li, C., Liu, Y., Chen, Z. (2023). Study of mechanical properties of micron polystyrene-toughened epoxy resin. Applied Sciences, 13(6): 3981. https://doi.org/10.3390/app13063981

[31] Guo, W., Zheng, Z., Li, W., Li, H., Zeng, F.Y., Mao, H.J. (2023). The cellular structure and toughness of hydrogenated styrene-butadiene block copolymer reinforced polypropylene foams. Polymers, 15(6): 1503. https://doi.org/10.3390/polym15061503

NOMENCLATURE

A	Cross-sectional area of the impact specimen, m²
E	Absorbed impact energy, J
$I.S.$	Impact strength, kJ·m⁻²
N	Sample number in substitution sequence (1-6), dimensionless
R_p	Distance from pendulum center of gravity to rotation axis, m
U	Impact energy absorbed during fracture, J
W	Pendulum weight, N
x	Substitution ratio of Zn or Cd in filler system, dimensionless
Ψ	Total filler weight fraction, wt% (dimensionless)

Greek Symbols

α	Pendulum fall angle (initial release angle), rad
β	Pendulum rise angle (final angle after impact), rad

Subscripts

Cd	Related to cadmium content
f	Filler phase (Zn, Cd, Te)
PS	Polystyrene matrix
Te	Related to tellurium content
Zn	Related to zinc content

Subscripts and Superscripts

x	Variable representing incremental substitution ratio

APPENDIX

All sample compositions for G1-G3 (Zn, Cd, Te %, PS %), matching the substitution steps described in Section 2.2.

Supplementary Material

To ensure transparency and reproducibility, the complete composition details of all prepared samples are listed in Table S1. This table shows the exact weight percentages of Zn, Cd, Te, and PS for each filler level (Ψ) and substitution step within Groups G1, G2, and G3.

Table S1. Compositions of the prepared composite samples in Groups G1–G3

Group	Weight Fraction (Ψ)	Sample No.	Composition (Filler + PS)
G1: (Zn–Te)/PS	Ψ1 = 4%	1	Zn 0% + Te 4% + PS 96%
		2	Zn 0.8% + Te 3.2% + PS 96%
		3	Zn 1.6% + Te 2.4% + PS 96%
		4	Zn 2.4% + Te 1.6% + PS 96%
		5	Zn 3.2% + Te 0.8% + PS 96%
		6	Zn 4% + Te 0% + PS 96%
	Ψ2 = 8%	1	Zn 0% + Te 8% + PS 92%
		2	Zn 1.6% + Te 6.4% + PS 92%
		3	Zn 3.2% + Te 4.8% + PS 92%
		4	Zn 4.8% + Te 3.2% + PS 92%
		5	Zn 6.4% + Te 1.6% + PS 92%
		6	Zn 8% + Te 0% + PS 92%
	Ψ3 = 12%	1	Zn 0% + Te 12% + PS 88%
		2	Zn 2.4% + Te 9.6% + PS 88%
		3	Zn 4.8% + Te 7.2% + PS 88%
		4	Zn 7.2% + Te 4.8% + PS 88%
		5	Zn 9.6% + Te 2.4% + PS 88%
		6	Zn 12% + Te 0% + PS 88%
G2: (Cd–Te)/PS	Ψ1 = 4%	1	Cd 0% + Te 4% + PS 96%
		2	Cd 0.8% + Te 3.2% + PS 96%
		3	Cd 1.6% + Te 2.4% + PS 96%

		4	Cd 2.4% + Te 1.6% + PS 96%
		5	Cd 3.2% + Te 0.8% + PS 96%
		6	Cd 4% + Te 0% + PS 96%
	Ψ2 = 8%	1	Cd 0% + Te 8% + PS 92%
		2	Cd 1.6% + Te 6.4% + PS 92%
		3	Cd 3.2% + Te 4.8% + PS 92%
		4	Cd 4.8% + Te 3.2% + PS 92%
		5	Cd 6.4% + Te 1.6% + PS 92%
		6	Cd 8% + Te 0% + PS 92%
	Ψ3 = 12%	1	Cd 0% + Te 12% + PS 88%
		2	Cd 2.4% + Te 9.6% + PS 88%
		3	Cd 4.8% + Te 7.2% + PS 88%
		4	Cd 7.2% + Te 4.8% + PS 88%
		5	Cd 9.6% + Te 2.4% + PS 88%
		6	Cd 12% + Te 0% + PS 88%
G3: (Zn–Cd–Te)/PS	Ψ1 = 6%	1	Zn 0% + Cd 4% + Te 2% + PS 94%
		2	Zn 0.8% + Cd 3.2% + Te 2% + PS 94%
		3	Zn 1.6% + Cd 2.4% + Te 2% + PS 94%
		4	Zn 2.4% + Cd 1.6% + Te 2% + PS 94%
		5	Zn 3.2% + Cd 0.8% + Te 2% + PS 94%
		6	Zn 4% + Cd 0% + Te 2% + PS 94%
	Ψ2 = 10%	1	Zn 0% + Cd 8% + Te 2% + PS 90%
		2	Zn 1.6% + Cd 6.4% + Te 2% + PS 90%
		3	Zn 3.2% + Cd 4.8% + Te 2% + PS 90%
		4	Zn 4.8% + Cd 3.2% + Te 2% + PS 90%
		5	Zn 6.4% + Cd 1.6% + Te 2% + PS 90%
		6	Zn 8% + Cd 0% + Te 2% + PS 90%
	Ψ3 = 14%	1	Zn 0% + Cd 12% + Te 2% + PS 86%
		2	Zn 2.4% + Cd 9.6% + Te 2% + PS 86%
		3	Zn 4.8% + Cd 7.2% + Te 2% + PS 86%
		4	Zn 7.2% + Cd 4.8% + Te 2% + PS 86%
		5	Zn 9.6% + Cd 2.4% + Te 2% + PS 86%
		6	Zn 12% + Cd 0% + Te 2% + PS 86%